THE JOURNAL OF PHYSICAL CHEMISTRY LETTERS
A JOURNAL OF THE AMERICAN CHEMICAL SOCIETY

pubs.acs.org/JPCL

Letter

Localized Spectroelectrochemical Identification of Basal Plane and Defect-Related Charge-Transfer Processes in Graphene

Martin Jindra, Matěj Velický,* Milan Bouša, Ghulam Abbas, Martin Kalbáč, and Otakar Frank*

Cite This: *J. Phys. Chem. Lett.* 2022, 13, 642−648

Read Online

ACCESS | Metrics & More | Article Recommendations | Supporting Information

ABSTRACT: It is well-known that structural defects play a decisive role in electrochemical behavior of atomically thin materials, where all the defects are directly accessible by the electrolyte. However, the vast majority of experimental techniques do not allow disentanglement of the processes at the edges/defects from those at the intact basal plane. Therefore, to address this issue, we introduce a localized spectroelectrochemical method featuring a microdroplet electrochemical cell with simultaneous Raman spectroscopy monitoring. The electrochemical and spectral responses of the basal planes of monolayer graphene samples with varying levels of disorder were compared. Two contributions, stemming from the intact and defective areas on the surface, respectively, were discovered both in the Raman G band shifts and cyclic voltammetry using the hexaammineruthenium complex. Consequently, two independent electron transfer processes of slower and faster rates coexist in one sample, but they are restricted to the defect-free and defect-rich areas, respectively.

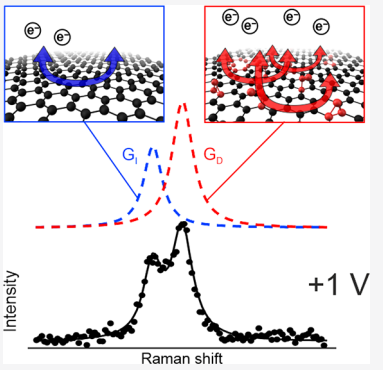

Research on two-dimensional (2D) materials is one of the most prominent current fields of study. The first 2D material discovered is graphene, which has earned a central place thanks to the number of unique phenomena it harbors.[1−3] Graphene represents an exceptional nanomaterial, which still continues to provide scientists with new surprise breakthroughs, although more than 15 years have passed since its discovery.[4]

It has become apparent that sample preparation has a substantial impact on graphene properties. The most common techniques for 2D materials' preparation are mechanical exfoliation from bulk crystals, chemical vapor deposition (CVD), and liquid-phase exfoliation.[5] The properties and processing requirements for graphene prepared *via* these methods greatly varies. For example, it is generally accepted that graphene mechanically exfoliated from natural graphite is of the highest crystalline quality but its production is hard to scale. In contrast, CVD graphene typically contains more grain boundaries and defects from the growth process, but it is relatively scalable. Furthermore, subsequent handling and/or treatment of samples introduce other factors, which affect graphene behavior and performance.

The sample preparation and treatment is particularly defining for the electrochemistry of graphene, which is extremely sensitive to adventitious contamination, surface type, and domain size.[6,7] Because the typical lateral dimensions of a single-crystal graphene are tens or hundreds of micrometers, macroscale electrochemical measurements yield a response averaged over many distinct surfaces. These variations in sample origin, history, and heterogeneity have led to markedly contradicting reports on fundamental electrochemistry of graphene. The best example of such a discrepancy is the dependence of the electron transfer kinetics on the number of graphene layers: increase, decrease, as well as independence were all argued for.[8−10] Sample heterogeneity can be efficiently tackled using a measurement in a microdroplet electrochemical cell (see scheme on Figure 1a), which facilitates electrochemical characterization or electrolyte gating of precisely defined surface regions.[11] This approach allows targeting of the basal plane versus edge plane regions or specific thickness with a micrometer precision.

Raman spectroscopy is the most utilized method for basic (thickness, disorder) as well as advanced (deformation, carrier concentration, *etc.*) characterization of graphene.[12−14] The introduction of the vector analysis of the positions of the G and 2D bands for the disentanglement of strain and charge doping has made Raman spectroscopy a particularly powerful tool, capable of delivering crucial information about the samples at a micrometer lateral resolution without resorting to more destructive or expensive techniques.[15,16] Uncomplicated implementation as an *in situ* method to monitor the material changes while imposing external perturbations (temperature, deformation, charge doping) is another advantage of Raman spectroscopy. In most of these experiments, the perturbation is

Received: October 22, 2021
Accepted: January 3, 2022
Published: January 12, 2022

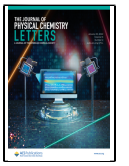

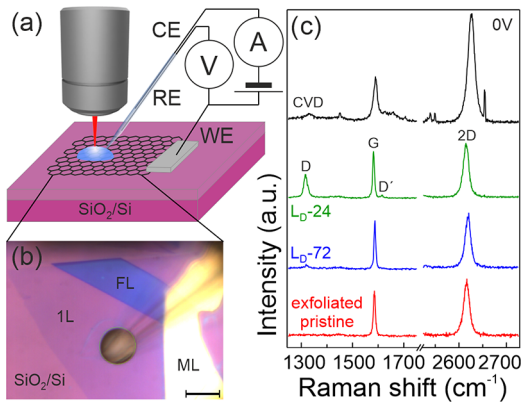

Figure 1. (a) Schematic of the Raman-μSEC setup. (b) An optical photograph showing the mono-, few-, and multilayer graphene areas (1L, FL, and ML, respectively) on an SiO_2/Si substrate investigated using a microdroplet. The scale bar corresponds to 10 μm. (c) Raman spectra of pristine exfoliated graphene, exfoliated graphene with defects introduced at average distances of 72 and 24 nm, and CVD graphene. The spectra were taken in the μ-droplet area with the set potential of 0 V (*vs* Ag/AgCl in 6 M LiCl). Spectra are normalized to the intensity of the G band.

inflicted globally. For example, although the phenomena of charge doping are known to be highly localized,[17,18] most of the *in situ* Raman experiments combined with electrolyte gating, conducted so far, have been done using large-area reservoirs of charge carriers covering the entire graphene sheet.[19−22] Hence, in such standard experiments, it is impossible to recognize the influence of localized defects (edges, vacancies, sp^3-hybridized carbon atoms) on the doping-induced changes in the Raman spectra.

We address these issues by employing localized Raman spectroelectrochemical measurements (Raman-μSEC) of the doping-dependent influence of defects on charge transfer in monolayer graphene. This method relies on application of voltage using a microdroplet electrochemical cell with a simultaneous spectroscopy measurement (μSEC). Both Raman spectroscopy and cyclic voltammetry (with a redox mediator) are able to distinguish the presence of surface types with different charge transfer rates depending on the absence or presence of structural defects.

We focus on the basal plane of graphene monolayers (Figure 1b). A microdroplet of 6 M LiCl (aq) with a typical diameter of ∼10−20 μm is placed inside the flake interior to interrogate its intrinsic (spectro)electrochemical behavior that is influenced by as low amount of structural defects (vacancies, grain boundaries, edges) and chemical contamination as possible. Such an approach can yield information previously inaccessible by conventional macroelectrochemistry on the routinely used CVD and transferred graphene.

Pristine exfoliated graphene, considered to be mostly devoid of defects,[23] exhibits two prominent Raman modes, G (corresponding to the zone-center phonon with E_{2g} symmetry, with the Raman shift, $\omega_G \sim 1580$ cm^{-1} for suspended graphene) and 2D ($\omega_{2D} \sim 2500$−2800 cm^{-1}; excitation wavelength-dependent) (Figure 1c).[12,14] Comparison of the pristine exfoliated graphene spectra with those of the exfoliated graphene with oxygen plasma-introduced defects and CVD graphene (all on a SiO_2/Si substrate), acquired using the Raman-μSEC at a potential of 0 V *vs* Ag/AgCl in 6 M LiCl

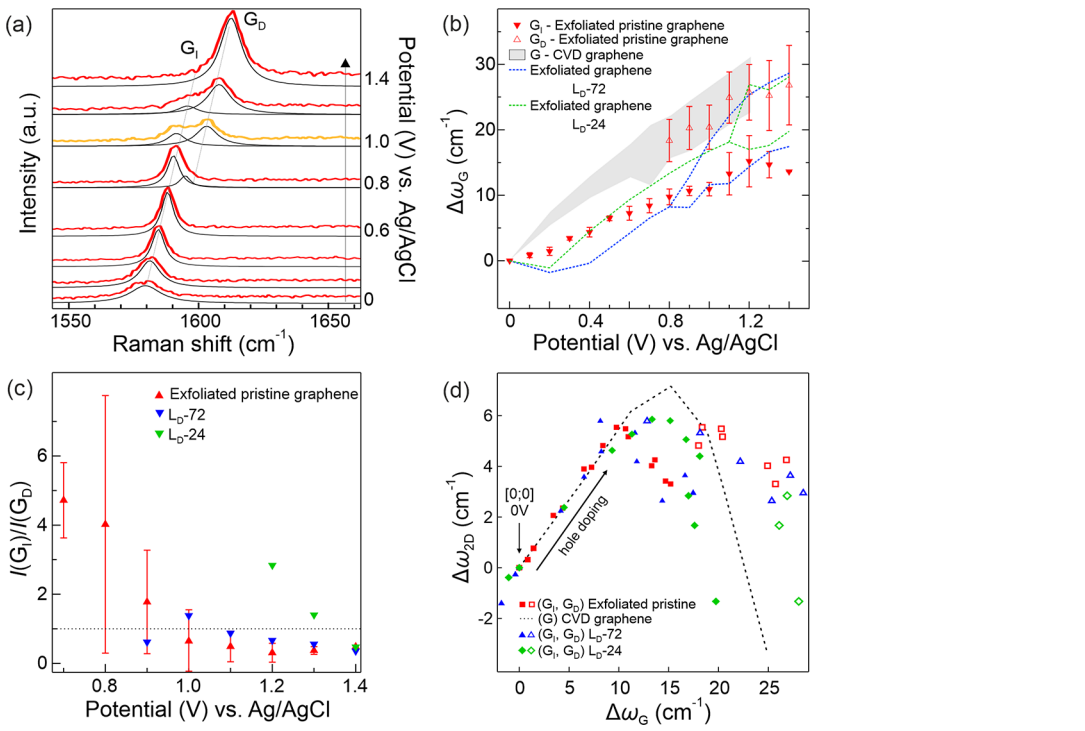

Figure 2. (a) Evolution of the Raman spectra of 1L pristine exfoliated graphene with the applied potential between 0 and 1.4 V *vs* Ag/AgCl in 6 M LiCl (0.2 V potential step). Black lines depict Lorentzian fits. (b) G band shift relative to its value at 0 V as a function of the applied potential (red error bars represent standard deviation from 3−8 measurements, gray shaded area of CVD graphene is the range defined by standard deviation from four measurements). (c) The $I(G_I)/I(G_D)$ intensity ratio as a function of the applied potential. (d) Correlation of the relative positions of the G and 2D modes for all the samples. Full and empty symbols denote the G_I and G_D sub-bands, respectively.

https://doi.org/10.1021/acs.jpclett.1c03466
J. Phys. Chem. Lett. 2022, 13, 642−648

(further referred to as *vs* Ag/AgCl), is shown in Figure 1c. Both the CVD and defective graphene Raman spectra feature additional D ($\omega_D \sim 1350$ cm^{-1}) and D′ ($\omega_{D'} \sim 1615$ cm^{-1}) modes, induced by the defects in the graphene lattice. The L_D-72 and L_D-24 samples were prepared by exposing the pristine exfoliated graphene to oxygen plasma of such levels, for which the average distance between individual defects in the lattice (L_D) corresponds to 72 and 24 nm, respectively (see Supporting Information for details).

All the Raman modes are strongly affected by the presence of strain and doping due to the high sensitivity of graphene to external perturbations.[13,19,24] The spectra of CVD and pristine exfoliated graphene are distinctly different. The larger variation in the shift and line width of both G and 2D modes of CVD graphene ensues from the growth-induced compression and doping by transfer process residues. Additionally, the larger heterogeneity of the CVD graphene is reflected in the peak broadening, larger even than for the L_D samples. The defects in the L_D samples are not well-defined as the plasma-induced vacancies are quickly functionalized by various oxygen-bearing groups.[25]

Figure 2a shows the evolution of the Raman G mode range of pristine exfoliated graphene upon stepwise application of electrochemical potential from 0 to 1.4 V (positive electrochemical potentials refer to hole doping, in contrast to the opposite voltage notation in dielectric gating). The G band shift indicates pure hole doping from 0 V up to 0.6 V (see also Figure 2d and related discussion). In the potential range of 0.6−0.8 V, the G band seemingly starts to split into two overlapping sub-bands, referred to herein as G_I and G_D. Importantly, we assign both of these sub-bands to the same E_{2g} phonon, however, we infer that they stem from the intact and defective graphene areas, respectively, and therefore reflect the heterogeneity of the electrolyte-gated surface. Initially, the intensity of G_I prevails, with the $I(G_I)/I(G_D)$ intensity ratio of ∼5 (Figure 2c). At ∼1 V, the two bands have similar intensities (orange spectrum in Figure 2a). For >1 V, the trend is reversed and $I(G_I)/I(G_D)$ drops below 1 as G_D becomes the prominent band.

Both sub-bands continue to blue-shift with the increasing hole concentration. The changes in the G mode positions, $\Delta\omega_G$, relative to ω_G at zero (0 V) potential, are plotted in Figure 2b for a comparison between individual samples. The G band of the 1L exfoliated graphene before the apparent splitting (full red triangles) shifts at a smaller rate with the applied potential compared to CVD graphene (gray shaded area), whose G mode does not split at any potential. The shift rates between 0.2 and 0.8 V are 13.9 cm^{-1} V^{-1} and 20.9 cm^{-1} V^{-1} for pristine exfoliated and CVD graphene, respectively. In the same potential range, the plasma-treated samples L_D-72 and L_D-24 shift by 16.7 cm^{-1} V^{-1} and 24.0 cm^{-1} V^{-1}, respectively. Interestingly, after the appearance of the two G bands in pristine exfoliated graphene, the positions of G_D (empty red triangles) fall exactly within the range of the CVD graphene shift, which suggests the importance of defects for the observed Raman spectroscopy response: *cf.* shift rates of 18.4 cm^{-1} V^{-1} for the G_D peak of pristine exfoliated graphene and 20.1 cm^{-1} V^{-1} for the G peak of CVD graphene, in the potential range of 0.8−1.2 V.

The Raman response of the two defective exfoliated samples falls in between that of pristine exfoliated and CVD graphene. Both the initial shift rate and the potential, at which the two G bands appear, are increasing with the increasing defect concentration. After the splitting, the sub-bands of both defective samples follow the same evolution as outlined for pristine and CVD graphene. Also, in all cases, the G_D band dominates the spectra at 1.4 V (Figure 2c). The spectra of the CVD graphene and both L_D samples are shown in the Supporting Information (SI)(Figures S1−S3).

Importantly, despite the differences in structural disorder and variations in the initial G band shift rates in the studied samples, the shifts of the G and 2D modes are induced solely by the applied potential, *i.e.*, by hole doping. Figure 2d shows the correlation of the relative G and 2D positions for all the samples. Such a plot enables us to discriminate the effects of strain and doping, which cause different shift rates of the G and 2D bands.[16] From the beginning of the experiment, up to the point of the appearance of the two G bands in the exfoliated samples, all data points in Figure 2d lie on the black dashed line corresponding to CVD graphene. This line's slope is 0.55, corresponding to pure hole doping.[16] Upon further increase of the potential, $\Delta\omega_{2D}$ starts to decrease, in agreement with previous reports.[19,20,22]

It is important to note that the observed behavior exhibits only a negligible hysteresis. Figure 3 shows the reversibility of the pristine exfoliated graphene spectra in the whole

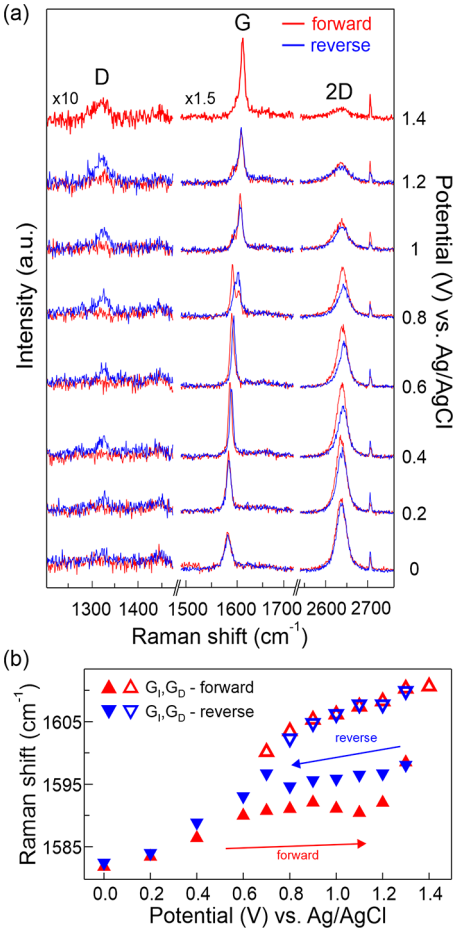

Figure 3. (a) Evolution of the Raman D, G, and 2D modes of 1L pristine exfoliated graphene during one complete spectroelectrochemical cycle. The forward (red spectra) and reverse (blue spectra) potential sweeps were carried out with steps of 0.2 V at low potentials and 0.1 V at high potentials. (b) Raman shift of the G_I and G_D sub-bands as a function of potential in one spectroelectrochemical cycle.

https://doi.org/10.1021/acs.jpclett.1c03466
J. Phys. Chem. Lett. 2022, 13, 642−648

voltammetric cycle from 0 to 1.4 V and back to 0 V. Only minor differences are observed in the relative intensities of the G bands, and their positions remain almost the same for a given potential. It can also be seen that a low intensity D band, activated by disorder, appears at potentials greater than ∼1.2 V, and its presence persists until the end of the experiment, albeit with a very low intensity. The disorder is connected to the (photo)electrochemical oxidation of the graphene surface, onset of which was reported in the potential range of 1.2−1.6 V *vs* standard hydrogen electrode (corresponding to 1.0−1.4 *vs* Ag/AgCl in 6 M LiCl used in our study) for natural graphite, CVD graphene, and glassy carbon.[26−28] No D′ band can be observed in the Raman spectra in Figure 3, as expected from the only low intensity of the D band.

We now turn the attention to the explanation of the observed Raman G band splitting, which has not yet been observed during either electrolyte or dielectric gating of 1L graphene. Importantly, we can support the validity of our methodology by comparing the results for CVD graphene with previous works (see SI for details).[19,20,29−32] We also performed polarized Raman spectroscopy measurements to rule out possible G band splitting due the symmetry breaking upon uniaxial deformation (see SI for details). The Raman shift, at which the G_D appears (∼1595 cm^{-1}), also precludes its assignment to the D′ mode. Moreover, the D′ band is known to exhibit only small frequency changes with doping,[21,31] whereas the G_D shifts at rates of ∼20 cm^{-1} V^{-1}. Finally, the G band splitting observed in the present work should not be interpreted as in the case of graphite intercalation, where the G band components originate from differently strained and charged graphene layers in the graphitic stack, depending on whether the intercalating ions entered the adjacent interlayer gallery or not.[33] A multilayer graphene/graphite sample is needed for such an observation.

The root cause of the observed splitting has to be looked for in the presence of defects and their distribution in the studied samples. Our experiments show a clear difference in the G band Raman shift per applied potential, in the order L_D-24 > CVD > L_D-72 > pristine exfoliated graphene. On top of that, the G band splits into two components at progressively higher potentials as a function of the defect density: pristine exfoliated < L_D-72 < L_D-24. No G band splitting was observed in CVD graphene.

It has been shown that contact resistance between graphene and metal contacts increases dramatically when defects are introduced into graphene before the metal deposition.[17,34] The high contact resistance of an electrical connection to basal plane graphene arises from its low density of electronic states (DOS), especially close to the Dirac point. The sheet resistance of graphene is lower than that of the metal and thus the carriers travel preferentially through the metal contact until an edge in the contact geometry, where they flow into graphene.[35] Consequently, patterning of graphene by etching holes into it results in lowering the contact resistance by increasing the total perimeter of the holes under the metal.[17] Lower contact resistance was also observed in graphene where the area under the metal was gently treated by oxygen plasma.[34]

We thus envisage the following scenario: in CVD graphene, the charge transfer proceeds predominantly through the existing defects and the contribution from the basal plane is negligible. In pristine exfoliated graphene, there is no possibility for the charge carriers to enter the graphene through the flake edges thanks to the localization of the μ-droplet experiment, as opposed to the previous macroscale experiments.[19,20,29−31] Hence, initially, the charge transfer proceeds only *via* the basal plane at a slower rate, reflected in the lower G band shift. With the increasing potential, defects are created and they start to contribute to a faster charge transfer and a larger local doping, manifested as the appearance of the G band component with a higher shift rate. However, large portions of the surface are still defect-free, which leads to a bimodal, slower and faster distribution of the charge transfer pathways. This spatial heterogeneity is, in turn, reflected in the appearance of the two G bands with lower and higher shift rate. At 1.3 V, the hole concentration in the defect-free and defect-rich surfaces can be estimated to 1.0×10^{13} cm^{-2} and 2.4×10^{13} cm^{-2}, respectively, upon comparison of the G_I and G_D Raman shifts with previously reported G band shifts.[20] Finally, the defect-driven charge transfer prevails over the basal plane processes at the highest potentials, where graphene oxidation takes place. In exfoliated graphene with oxygen plasma-induced defects, the faster charge transfer is already visible from lower potentials, while the bimodal distribution of the regions with the different processes becomes apparent only at higher potentials, where the two G components are more separated.

In support of the spectroelectrochemistry results, we assessed the electron transfer activity of the different graphene samples using the hexaammineruthenium complex, $[Ru(NH_3)_6]^{3+/2+}$. $[Ru(NH_3)_6]^{3+/2+}$ is an outer-sphere redox mediator, whose response is sensitive to the electronic structure of the electrode and whose rate of electron transfer therefore directly reflects the DOS of graphene. Figure 4a−d show cyclic voltammograms of the $[Ru(NH_3)_6]^{3+/2+}$ reduction/oxidation on the four different graphene surfaces at scan rates varied from 0.75 to 3.5 V s^{-1}. Cyclic voltammograms on pristine exfoliated graphene in Figure 4a exhibit the expected increase of the peak-to-peak separation (ΔE) of the oxidation and reduction reactions with scan rate.[36] Similar orderly dependence of ΔE on scan rate is found for CVD graphene in Figure 4d. This textbook behavior allows for a straightforward determination of the standard heterogeneous electron transfer rate constant (k^0), which decreases with increasing ΔE for a given scan rate.

In contrast, behavior of the two defective graphene samples (Figure 4b,c), particularly for the oxidation part of the voltammogram, is more complex. The initially small ΔE (indicating fast electron transfer) of the first recorded voltammogram at 3.5 V s^{-1}, increases for the subsequent voltammograms at smaller scan rates, in particular for the L_D-76 graphene (Figure 4c). This is contrary to the expected decrease of ΔE with the decreasing scan rate and indicates a temporal dependence of k^0. It is likely that this drop in the electron transfer rate follows an irreversible electrochemical reduction of the oxygenated functional groups created by the oxygen plasma, which initially mediate fast electron transfer. Starting from the scan rate of 2.5 V s^{-1}, the oxidation branches of the L_D-76 and L_D-120 graphene voltammograms contain two components with a differing rate of dependence on the scan rate. This reveals the existence of two independent electron transfer processes arising from two types of graphene surfaces with differing DOS, and therefore k^0. The resulting scan rate-dependent shape of the voltammograms is the product of the diffusional overlap between the "faster" and "slower" surface domains, which was described theoretically

https://doi.org/10.1021/acs.jpclett.1c03466
J. Phys. Chem. Lett. 2022, 13, 642−648

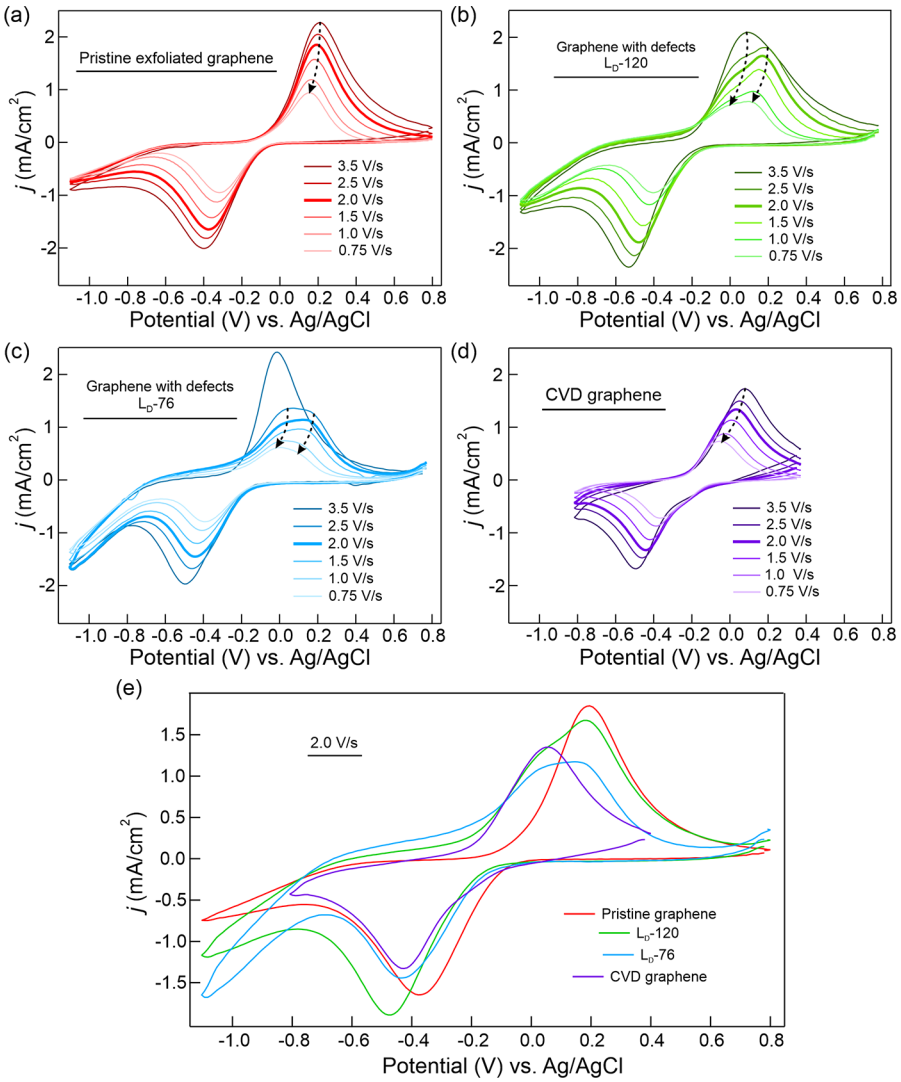

Figure 4. Cyclic voltamograms recorded with different scan rates in a microdroplet solution of 2 mM $[Ru(NH_3)_6]Cl_3$ in 6 M LiCl (aq): (a) pristine exfoliated graphene, (b) exfoliated graphene with defects made by oxygen plasma, L_D = 120 nm, (c) exfoliated graphene with defects made by oxygen plasma, L_D = 76 nm, and (d) CVD graphene. (e) comparison of voltammograms for all four graphene types at a single scan rate 2 V s^{-1}.

using finite difference simulations[37] and recently confirmed experimentally for graphite.[26]

The most plausible reason for the "well-behaved" ΔE-scan rate dependence of the pristine exfoliated and CVD graphene is the uniformity of the surface at a scale relevant to the voltammetric measurement: pristine exfoliated graphene is predominantly composed of the defect-free basal plane with only a small number of uniformly distributed defects, while CVD graphene is predominantly composed of a dense patchwork of basal plane domains connected by grain boundaries. This results in an averaged electrochemical response because the individual surface types (basal plane, defects, grain boundaries) are distributed too uniformly to be resolved in a voltammetric experiment.

Cyclic voltammograms for all graphene types at 2 V s^{-1} are shown in Figure 4e. This comparison corroborates the general understanding of the electron transfer kinetics on graphene/graphite: the defect-free basal plane, approximated here by the pristine exfoliated graphene with k^0 of 0.8×10^{-4} cm s^{-1} has slower kinetics than defected surfaces, approximated here by the CVD graphene with k^0 of 1.8×10^{-4} cm s^{-1}. As discussed above, the oxidation voltammetric branches of the defective graphene samples are dominated not by one, but two separate processes corresponding to surfaces with "faster" and "slower" electron transfer kinetics. Interestingly, while the "faster" k^0 values (1.9×10^{-4} cm s^{-1} for L_D-76 and 1.3×10^{-4} cm s^{-1} L_D-120) are in a similar range as the 1.8×10^{-4} cm s^{-1} for CVD graphene, the "slower" k^0 values are much more scattered (*cf.* 0.4×10^{-4} cm s^{-1} for L_D-76, 0.2×10^{-4} cm s^{-1} for L_D-120, and 0.8×10^{-4} cm s^{-1} for pristine graphene). This suggests that it is difficult to isolate the electrochemical response of a truly pristine basal plane. Instead, even the pristine exfoliated graphene very likely contains nanoscale defects, whose high electrochemical activities affect the resulting k^0. Note, however, that the differences in the absolute value of k^0 are not large enough for firm conclusions to be drawn, which reflects the literature controversy of contrasting views on the electron transfer activity of the basal plane, defects, edges, and grain boundaries of graphene/graphite.[38−42]

We introduce a novel Raman-μSEC method, which allows for a simultaneous electrochemical and Raman spectroscopy investigation at the micrometer lateral scale, without the need for lithographic processes contaminating the sample surface. We applied this method to elucidate the doping-dependent

https://doi.org/10.1021/acs.jpclett.1c03466
J. Phys. Chem. Lett. 2022, 13, 642−648

influence of structural defects on the electrochemical phenomena at the otherwise defect-free basal plane of monolayer graphene. We discovered the presence of two distinct types of surfaces, which coexist even within the area delimited by the microscale dimensions of the electrochemical cell and the laser spot. The differing behavior of the two surface types manifests in the Raman spectral response by an apparent G band splitting with the applied potential, as well as in the cyclic voltammograms using an outer-sphere redox mediator. Both observations point to different charge transfer processes with varying rates, which take place at the defect-free and defect-rich regions at the surface. Our results highlight the necessity of using localized methods when assessing the (spectro)electrochemical properties of materials with a distinctly heterogeneous surface morphology.

■ ASSOCIATED CONTENT

Supporting Information

The Supporting Information is available free of charge at https://pubs.acs.org/doi/10.1021/acs.jpclett.1c03466.

Experimental methods, potential-dependent evolution of Raman spectra of CVD graphene and exfoliated graphene samples with plasma-induced defects, additional Raman analyses (PDF)

■ AUTHOR INFORMATION

Corresponding Authors

Otakar Frank − *J. Heyrovský Institute of Physical Chemistry, Czech Academy of Sciences, 182 23 Prague, Czech Republic;* orcid.org/0000-0002-9661-6250; Email: otakar.frank@jh-inst.cas.cz

Matěj Velický − *J. Heyrovský Institute of Physical Chemistry, Czech Academy of Sciences, 182 23 Prague, Czech Republic; Department of Physics and Astronomy, University of Manchester, M13 9PL Manchester, United Kingdom;* orcid.org/0000-0003-4230-3811; Email: matej.velicky@jh-inst.cas.cz

Authors

Martin Jindra − *J. Heyrovský Institute of Physical Chemistry, Czech Academy of Sciences, 182 23 Prague, Czech Republic; Department of Physical Chemistry, University of Chemistry and Technology, 16628 Prague, Czech Republic;* orcid.org/0000-0002-3396-8830

Milan Bouša − *J. Heyrovský Institute of Physical Chemistry, Czech Academy of Sciences, 182 23 Prague, Czech Republic;* orcid.org/0000-0002-1073-7386

Ghulam Abbas − *J. Heyrovský Institute of Physical Chemistry, Czech Academy of Sciences, 182 23 Prague, Czech Republic; Department of Physical Chemistry and Macromolecular Chemistry, Faculty of Science, Charles University in Prague, 128 43 Prague 2, Czech Republic*

Martin Kalbáč − *J. Heyrovský Institute of Physical Chemistry, Czech Academy of Sciences, 182 23 Prague, Czech Republic;* orcid.org/0000-0001-9574-4368

Complete contact information is available at: https://pubs.acs.org/10.1021/acs.jpclett.1c03466

Notes

The authors declare no competing financial interest.

■ ACKNOWLEDGMENTS

This work was funded by the Czech Science Foundation (GACR 20-08633X). M.B. acknowledges the support by European Regional Development Fund; OP RDE; Project: "Carbon allotropes with rationalized nanointerfaces and nanolinks for environmental and biomedical applications" (no. CZ.02.1.01/0.0/0.0/16_026/0008382), and G.A. thanks the Charles University Grant Agency (GAUK, project no. 371621)

■ REFERENCES

(1) Bolotin, K. I.; Sikes, K. J.; Jiang, Z.; Klima, M.; Fudenberg, G.; Hone, J.; Kim, P.; Stormer, H. L. Ultrahigh Electron Mobility in Suspended Graphene. *Solid State Commun.* **2008**, *146*, 351−355.

(2) Nair, R. R.; Blake, P.; Grigorenko, A. N.; Novoselov, K. S.; Booth, T. J.; Stauber, T.; Peres, N. M. R.; Geim, A. K. Fine Structure Constant Defines Visual Transparency of Graphene. *Science* **2008**, *320*, 1308.

(3) Novoselov, K. S.; Geim, A. K.; Morozov, S. V.; Jiang, D.; Katsnelson, M. I.; Grigorieva, I. V.; Dubonos, S. V.; Firsov, A. A. Two-Dimensional Gas of Massless Dirac Fermions in Graphene. *Nature* **2005**, *438*, 197−200.

(4) Ku, M. J. H.; Zhou, T. X.; Li, Q.; Shin, Y. J.; Shi, J. K.; Burch, C.; Anderson, L. E.; Pierce, A. T.; Xie, Y.; Hamo, A.; et al. Imaging Viscous Flow of the Dirac Fluid in Graphene. *Nature* **2020**, *583*, 537−541.

(5) Bonaccorso, F.; Lombardo, A.; Hasan, T.; Sun, Z.; Colombo, L.; Ferrari, A. C. Production and Processing of Graphene and 2d Crystals. *Mater. Today* **2012**, *15*, 564−589.

(6) Patten, H. V.; Velický, M.; Clark, N.; Muryn, C. A.; Kinloch, I. A.; Dryfe, R. A. W. Electrochemistry of Well-Defined Graphene Samples: Role of Contaminants. *Faraday Discuss.* **2014**, *172*, 261−271.

(7) Kislenko, V. A.; Pavlov, S. V.; Kislenko, S. A. Influence of Defects in Graphene on Electron Transfer Kinetics: The Role of the Surface Electronic Structure. *Electrochim. Acta* **2020**, *341*, 136011.

(8) Güell, A. G.; Ebejer, N.; Snowden, M. E.; MacPherson, J. V.; Unwin, P. R. Structural Correlations in Heterogeneous Electron Transfer at Monolayer and Multilayer Graphene Electrodes. *J. Am. Chem. Soc.* **2012**, *134*, 7258−7261.

(9) Valota, A. T.; Kinloch, I. A.; Novoselov, K. S.; Casiraghi, C.; Eckmann, A.; Hill, E. W.; Dryfe, R. A. W. Electrochemical Behavior of Monolayer and Bilayer Graphene. *ACS Nano* **2011**, *5*, 8809−8815.

(10) Goh, M. S.; Pumera, M. The Electrochemical Response of Graphene Sheets Is Independent of the Number of Layers from a Single Graphene Sheet to Multilayer Stacked Graphene Platelets. *Chem.-Asian J.* **2010**, *5*, 2355−2357.

(11) Velický, M.; Bradley, D. F.; Cooper, A. J.; Hill, E. W.; Kinloch, I. A.; Mishchenko, A.; Novoselov, K. S.; Patten, H. V.; Toth, P. S.; Valota, A. T.; et al. Electron Transfer Kinetics on Mono- and Multilayer Graphene. *ACS Nano* **2014**, *8*, 10089−10100.

(12) Ferrari, A. C.; Meyer, J. C.; Scardaci, V.; Casiraghi, C.; Lazzeri, M.; Mauri, F.; Piscanec, S.; Jiang, D.; Novoselov, K. S.; Roth, S.; et al. Raman Spectrum of Graphene and Graphene Layers. *Phys. Rev. Lett.* **2006**, *97*, 187401.

(13) Ferrari, A. C.; Basko, D. M. Raman Spectroscopy as a Versatile Tool for Studying the Properties of Graphene. *Nat. Nanotechnol.* **2013**, *8*, 235−246.

(14) Malard, L. M.; Pimenta, M. A.; Dresselhaus, G.; Dresselhaus, M. S. Raman Spectroscopy in Graphene. *Phys. Rep.* **2009**, *473*, 51−87.

(15) Lee, J. E.; Ahn, G.; Shim, J.; Lee, Y. S.; Ryu, S. Optical Separation of Mechanical Strain from Charge Doping in Graphene. *Nat. Commun.* **2012**, *3*, 1024.

(16) Mueller, N. S.; Heeg, S.; Peña-Alvarez, M.; Kusch, P.; Wasserroth, S.; Clark, N.; Schedin, F.; Parthenios, J.; Papagelis, K.; Galiotis, C.; et al. Evaluating Arbitrary Strain Configurations and

Doping in Graphene with Raman Spectroscopy. *2D Mater.* **2018**, *5*, No. 015016.
(17) Passi, V.; Gahoi, A.; Marin, E. G.; Cusati, T.; Fortunelli, A.; Iannaccone, G.; Fiori, G.; Lemme, M. C. Ultralow Specific Contact Resistivity in Metal−Graphene Junctions Via Contact Engineering. *Adv. Mater. Interfaces* **2019**, *6*, 1801285.
(18) Martin, J.; Akerman, N.; Ulbricht, G.; Lohmann, T.; Smet, J. H.; von Klitzing, K.; Yacoby, A. Observation of Electron-Hole Puddles in Graphene Using a Scanning Single-Electron Transistor. *Nat. Phys.* **2008**, *4*, 144−148.
(19) Frank, O.; Dresselhaus, M. S.; Kalbac, M. Raman Spectroscopy and in Situ Raman Spectroelectrochemistry of Isotopically Engineered Graphene Systems. *Acc. Chem. Res.* **2015**, *48*, 111−118.
(20) Das, A.; Pisana, S.; Chakraborty, B.; Piscanec, S.; Saha, S. K.; Waghmare, U. V.; Novoselov, K. S.; Krishnamurthy, H. R.; Geim, A. K.; Ferrari, A. C.; et al. Monitoring Dopants by Raman Scattering in an Electrochemically Top-Gated Graphene Transistor. *Nat. Nanotechnol.* **2008**, *3*, 210−215.
(21) Bruna, M.; Ott, A. K.; Ijäs, M.; Yoon, D.; Sassi, U.; Ferrari, A. C. Doping Dependence of the Raman Spectrum of Defected Graphene. *ACS Nano* **2014**, *8*, 7432−7441.
(22) Froehlicher, G.; Berciaud, S. Raman Spectroscopy of Electrochemically Gated Graphene Transistors: Geometrical Capacitance, Electron-Phonon, Electron-Electron, and Electron-Defect Scattering. *Phys. Rev. B* **2015**, *91*, 205413.
(23) Banhart, F.; Kotakoski, J.; Krasheninnikov, A. V. Structural Defects in Graphene. *ACS Nano* **2011**, *5*, 26−41.
(24) Galiotis, C.; Frank, O.; Koukaras, E. N.; Sfyris, D. Graphene Mechanics: Current Status and Perspectives. *Annu. Rev. Chem. Biomol. Eng.* **2015**, *6*, 121−140.
(25) Li, H.; Singh, A.; Bayram, F.; Childress, A. S.; Rao, A. M.; Koley, G. Impact of Oxygen Plasma Treatment on Carrier Transport and Molecular Adsorption in Graphene. *Nanoscale* **2019**, *11*, 11145−11151.
(26) Velický, M.; Toth, P. S.; Woods, C. R.; Novoselov, K. S.; Dryfe, R. A. W. Electrochemistry of the Basal Plane versus Edge Plane of Graphite Revisited. *J. Phys. Chem. C* **2019**, *123*, 11677−11685.
(27) Li, W.; Wojcik, M.; Xu, K. Optical Microscopy Unveils Rapid, Reversible Electrochemical Oxidation and Reduction of Graphene. *Nano Lett.* **2019**, *19*, 983−989.
(28) Yi, Y.; Weinberg, G.; Prenzel, M.; Greiner, M.; Heumann, S.; Becker, S.; Schlögl, R. Electrochemical Corrosion of a Glassy Carbon Electrode. *Catal. Today* **2017**, *295*, 32−40.
(29) Kalbac, M.; Reina-Cecco, A.; Farhat, H.; Kong, J.; Kavan, L.; Dresselhaus, M. S. The Influence of Strong Electron and Hole Doping on the Raman Intensity of Chemical Vapor-Deposition Graphene. *ACS Nano* **2010**, *4*, 6055−6063.
(30) Chen, C.-F.; Park, C.-H.; Boudouris, B. W.; Horng, J.; Geng, B.; Girit, C.; Zettl, A.; Crommie, M. F.; Segalman, R. A.; Louie, S. G.; et al. Controlling Inelastic Light Scattering Quantum Pathways in Graphene. *Nature* **2011**, *471*, 617−620.
(31) Inukai, D.; Koyama, T.; Kawahara, K.; Ago, H.; Kishida, H. Electronic States of Electrochemically Doped Single-Layer Graphene Probed through Fano Resonance Effects in Raman Scattering. *J. Phys. Chem. C* **2020**, *124*, 26428−26433.
(32) Zhong, J.-H.; Liu, J.-Y.; Li, Q.; Li, M.-G.; Zeng, Z.-C.; Hu, S.; Wu, D.-Y.; Cai, W.; Ren, B. Interfacial Capacitance of Graphene: Correlated Differential Capacitance and in Situ Electrochemical Raman Spectroscopy Study. *Electrochim. Acta* **2013**, *110*, 754−761.
(33) Chacón-Torres, J. C.; Wirtz, L.; Pichler, T. Manifestation of Charged and Strained Graphene Layers in the Raman Response of Graphite Intercalation Compounds. *ACS Nano* **2013**, *7*, 9249−9259.
(34) Robinson, J. A.; LaBella, M.; Zhu, M.; Hollander, M.; Kasarda, R.; Hughes, Z.; Trumbull, K.; Cavalero, R.; Snyder, D. Contacting Graphene. *Appl. Phys. Lett.* **2011**, *98*, No. 053103.
(35) Nagashio, K.; Nishimura, T.; Kita, K.; Toriumi, A. Contact Resistivity and Current Flow Path at Metal/Graphene Contact. *Appl. Phys. Lett.* **2010**, *97*, 143514.
(36) Bard, A. J.; Faulkner, L. R. *Electrochemical Methods. Fundamentals and Applications*, 2nd ed.; John Wiley & Sons: New York, 2001; p 833.
(37) Davies, T. J.; Moore, R. R.; Banks, C. E.; Compton, R. G. The Cyclic Voltammetric Response of Electrochemically Heterogeneous Surfaces. *J. Electroanal. Chem.* **2004**, *574*, 123−152.
(38) McCreery, R. L.; Cline, K. K.; McDermott, C. A.; McDermott, M. T. Control of Reactivity at Carbon Electrode Surfaces. *Colloids Surf., A* **1994**, *93*, 211−219.
(39) Davies, T. J.; Hyde, M. E.; Compton, R. G. Nanotrench Arrays Reveal Insight into Graphite Electrochemistry. *Angew. Chem., Int. Ed.* **2005**, *44*, 5121−5126.
(40) Lai, S. C. S.; Patel, A. N.; McKelvey, K.; Unwin, P. R. Definitive Evidence for Fast Electron Transfer at Pristine Basal Plane Graphite from High-Resolution Electrochemical Imaging. *Angew. Chem., Int. Ed.* **2012**, *51*, 5405−5408.
(41) Zhong, J.-H.; Zhang, J.; Jin, X.; Liu, J.-Y.; Li, Q.; Li, M.-H.; Cai, W.; Wu, D.-Y.; Zhan, D.; Ren, B. Quantitative Correlation between Defect Density and Heterogeneous Electron Transfer Rate of Single Layer Graphene. *J. Am. Chem. Soc.* **2014**, *136*, 16609−16617.
(42) Jiang, L.; Fu, W.; Birdja, Y. Y.; Koper, M. T. M.; Schneider, G. F. Quantum and Electrochemical Interplays in Hydrogenated Graphene. *Nat. Commun.* **2018**, *9*, 793.

https://doi.org/10.1021/acs.jpclett.1c03466
J. Phys. Chem. Lett. 2022, 13, 642−648